

# A Numerical Study of Void Interactions in Elastic–Plastic Solids Containing Two-Scale Voids



A. K. Dwivedi, I. A. Khan, and J. Chattopadhyay

**Abstract** Ductile fracture in metals occurs due to the nucleation, growth and coalescence of microscopic voids, resulting in a macroscopic crack. These voids often originate at different length scales due to cracking of large-sized inclusions or decohesion at second-phase particles. In several structural materials like low-alloy steels, secondary voids accelerate the ductile damage process, thus, resulting in a severe reduction in ductility. A systematic study analyzing the effect of spatial distribution of secondary voids on the growth and coalescence of primary voids has yet not been reported. In the present work, finite element-based cell model studies are carried out to understand the void interactions in elastic–plastic solids containing voids at two distinct length scales. A double periodic array of primary and secondary voids subjected to uniaxial loading under plane strain condition is analyzed. The effect of secondary void location and its orientation on the mesoscale response and evolution of porosity is studied numerically. Our numerical results suggest that the interactions between the two-scale voids accelerate the growth and coalescence of primary voids.

**Keywords** Ductile fracture · Voids · Elastic–plastic solids · Finite element analysis

## Nomenclature

$2A_0$	Intervoid distance of primary voids in $X_1$ direction in undeformed state
$2B_0$	Intervoid distance of primary voids in $X_2$ direction in undeformed state
$D_{P0}$	Initial diameter of primary void
$D_{S0}$	Initial diameter of secondary void
$a_0$	Undeformed radius of primary void in $X_1$ direction
$c_0$	Undeformed radius of primary void in $X_2$ direction

---

A. K. Dwivedi (✉) · I. A. Khan · J. Chattopadhyay  
Homi Bhabha National Institute, Mumbai 400094, India  
e-mail: [akdwivedi@barc.gov.in](mailto:akdwivedi@barc.gov.in)

I. A. Khan · J. Chattopadhyay  
Reactor Safety Division, Bhabha Atomic Research Center, Mumbai 400085, India

P	Distance between primary and secondary void
$\theta_0$	Angle between secondary void and $X_1$ direction in the undeformed state
$\sigma_y$	Yield strength
E	Young's modulus
$\nu$	Poisson's ratio
n	Hardening exponent
$\sigma_e$	Equivalent stress
$\sigma_h$	Hydrostatic stress
T	Stress triaxiality ratio
$E_e$	Equivalent strain
VVF	Void Volume Fraction
$F_p$	Primary void volume fraction
$F_s$	Secondary void volume fraction
$F_T$	Total void volume fraction
$F_{p0}$	Initial volume fraction of primary void
$F_{s0}$	Initial volume fraction of secondary void
$V_0, V$	Initial and current volume of the cell, respectively

## 1 Introduction

Ductile fracture in metals comprises a three-stage process namely; void nucleation, growth and coalescence [1]. In structural metals like low-alloy steels, voids typically nucleate at different length scales due to cracking of large-sized inclusions or decohesion at second-phase particles. The larger-sized (primary) voids nucleate relatively early and enlarge due to plastic deformation of the surrounding matrix up to a point where plasticity localizes in the ligament between neighbouring voids [2, 3]. This stage is often referred to as the onset of void coalescence. Beyond this stage, primary voids typically link up to each other or to a main crack due to new surfaces created by nucleation, growth and coalescence of much smaller (secondary) voids that nucleate at relatively large strains [2]. Typically, secondary voids are defined as being one order of magnitude smaller than primary voids. The volume fraction of these secondary voids can be of the order of 1%. Experimental evaluation of the effect of secondary voids on the growth and coalescence of primary voids and, hence, on macroscopic ductility poses several challenges [2].

It is generally agreed that the mechanism of fracture in ductile materials is a manifestation of the role played by void population attributes, namely porosity, shape of voids and their spatial distribution (location and orientation), and the matrix hardening attributes in the mechanism of plastic flow and localization. The existing models of ductile fracture, however, have mainly focussed on the role of primary voids in the macroscopic fracture process. The development of these models is motivated by the seminal work of McClintock [4] and Rice and Tracey [5], who analyzed the growth of an isolated void in an infinite medium. Later, Gurson [6, 7] performed

a limit-analysis of a hollow sphere of finite radius, thus, incorporating the effect of arbitrary non-zero porosities on the macroscopic response of a rigid-plastic solid. The model was extended to include the effect of matrix hardening in a heuristic manner. Since the Gurson model accounted only for the void growth, heuristic corrections were incorporated to account for the mechanism of void nucleation and coalescence, notably based on micromechanical cell model studies. In recent years, an increasing attention has been paid to improved characterization of ductile fracture at low stress triaxiality [8]. Various generalizations of the Gurson model have been proposed to account for the anisotropies associated with plastic deformation of the matrix and the evolution of void shapes at arbitrary finite strains [10]. The existing ductile fracture models (including the recent ones which account for the anisotropic effects of matrix deformations and void shapes, as well as those based on rigorous nonlinear bounds), were developed on the basis that the void growth is driven by some diffuse plastic flow in the matrix. Consequently, predictions based on these models overestimate measured ductilities [2, 3]. Experimental observations suggest strong evidence for a termination to stable void growth by various mechanisms of flow localization in the intervoid matrix. An important contribution to the modelling of internal necking was made by Koplik and Needleman [11]. Void coalescence can also occur due to formation of a micro shear band between the neighbouring voids. Material instability inside this band is described by the localization condition proposed by Rice [12] and Needleman and Rice [13]. These studies, however, were focused on modelling the flow localization in a matrix containing only one population of void nucleating particles.

Although the role played by secondary voids in the macroscopic fracture process is well-recognized, till date only limited studies have focussed on modelling their effects on the fracture ductility. Perrin and Leblond [14] analyzed a hollow sphere containing one large primary void surrounded by a porous plastic matrix containing the secondary voids. Brocks et al. [15] and Fabregue and Pardoen [16] numerically modelled the effect of second population of voids using a Gurson-type model. Gao and Kim [17] proposed to account for the secondary voids through calibration of a critical porosity for the coalescence of primary voids. Faleskog and Shih [18], and Tvergaard [19, 20] carried out numerical studies with an explicit representation of both primary and secondary voids. These studies were focused on analyzing the role of increased local stresses resulting from the growth of larger voids in a cavitation type instability at the smaller void. The effect of void volume fraction on the void growth rate was studied numerically. While the former authors performed plane strain analysis of cylindrical voids, the later author carried out axi-symmetric studies on a special void configuration where each larger void was surrounded by a smaller void and vice-versa. More recent research in this area has focused on bringing the size effects of the secondary voids, [21–25] for a fixed volume fraction, on ductile fracture. While Zymbell et al. [25] performed cell model studies, Hutter et al. [24] focused on modelling the process zone near the crack tip. In both these studies, the primary voids were modelled discretely, and the size of the secondary voids was incorporated indirectly in terms of an intrinsic length that was introduced in the non-local formulation of the GTN model.

Most of the above-mentioned studies, employing a homogenized representation of the secondary voids, suggest that the nucleation and growth of secondary voids mainly accelerate the void coalescence process, the primary void growth is largely uninfluenced [16]. Based on an explicit representation of primary and secondary voids, Khan and Bhasin [26] have shown that the secondary voids can enhance the growth of primary voids and the mesoscopic ductility depends on the spatial distribution of secondary voids. In the present work, the effect of location and orientation of a secondary void, in the intervoid ligament between the primary voids, on the mesoscopic response and evolution of porosity is studied numerically. In particular, focus is laid on understanding how the voids originating at two distinct length scales interact with each other. Both the primary and secondary voids are assumed to be present from right from the beginning of the deformation history. Plane strain condition is assumed, and a uniaxial tensile load is applied. Our numerical results suggest that the interactions between the two-scale voids accelerate the growth and, hence, the coalescence of primary voids.

## 2 Problem Formulation

An elastic–plastic solid containing pre-existing voids of two different sizes is analyzed numerically. 2D double periodic arrays containing cylindrical primary and secondary voids are shown in Fig. 1. The diameters of primary and secondary voids, in the undeformed state, are denoted as  $D_{po}$  and  $D_{so}$ , respectively. The initial spacing

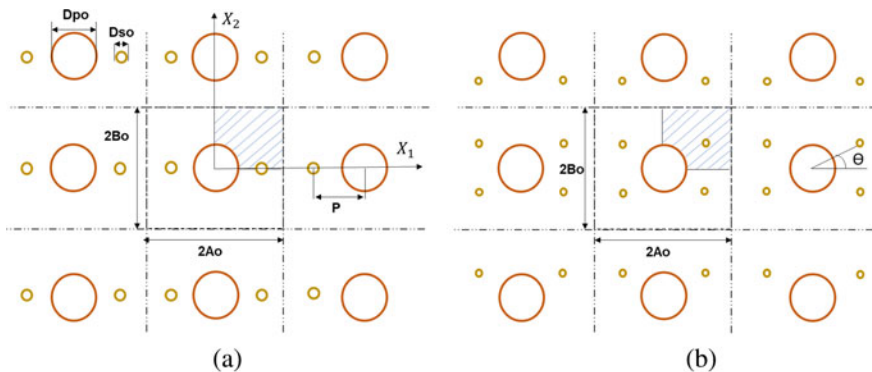


**Fig. 1** 2D double periodic arrays of primary and secondary voids analyzed in this study **a** two secondary voids are located in the intervoid ligament between the two primary voids **b** four secondary voids surround each primary void. Dashed square is showing a unit cell and the hatched portions are analyzed due to symmetry conditions. The initial volume fraction of primary and secondary voids is kept the same in (a) and (b)

between the two primary (large sized) voids is  $2A_0$  and  $2B_0$  in the  $X_1$  and  $X_2$  directions, respectively. Two different spatial distributions of secondary voids are considered. In Fig. 1a, two secondary voids are located in the intervoid ligament between the two primary voids. In the undeformed state, the distance of a secondary void from the neighbouring primary void is denoted by  $P$ . Figure 1b depicts an arrangement where four secondary voids surround each primary void and are lying at a fixed distance  $P$  from the neighbouring primary void. The initial orientation of a secondary void with respect to the intervoid ligament is described by the angle  $\theta$ . A uniaxial tensile load is applied at  $X_2 = B_0$ . The initial volume fraction of the secondary voids is kept the same for the two different voids arrangements, shown in Fig. 1.

### 2.1 Governing Equations

A Lagrangian finite strain formulation of the field equations is used. The initial unstressed state is taken as the reference configuration and the position of a material point, relative to a fixed Cartesian frame, in the reference configuration is denoted as  $x$ . The material point, initially at  $x$ , is at  $\bar{x}$  in the current configuration. The displacement vector  $u$  and the deformation gradient  $F$  are defined as

$$u = \bar{x} - x, F = \frac{\partial \bar{x}}{\partial x} \tag{1}$$

The finite element formulation is based on the principle of virtual work written as

$$\int_v s : \delta F dV = \int_s T \cdot \delta u dS \tag{2}$$

where  $s$  is the (nonsymmetric) nominal stress,  $T$  is the traction,  $u$  is the displacement,  $V$  and  $S$  are, respectively, the volume and surface of the body in the reference configuration. The traction and the reference configuration normal are related by  $T = n \cdot s$  and  $s = F^{-1} \tau$  with  $\tau = \det(F)\sigma$  and  $\sigma$  the Cauchy stress.

Due to symmetry considerations only 1/4th models, shown by hatched lines in Fig. 1, are analyzed numerically. Symmetry conditions are incorporated using the following boundary conditions,

$$u_1 = 0 \text{ at } x_1 = 0 \tag{3}$$

$$u_2 = 0 \text{ at } x_2 = 0 \tag{4}$$

The boundary of the cell model at  $x_1 = A_0$  is constrained to remain plane throughout the loading history to simulate periodic boundary condition. Plane strain condition is simulated by constraining the nodal displacements, that is,

$$u_3 = 0 \text{ at } x_3 = 0 \text{ and } x_3 = 1 \quad (5)$$

## 2.2 Constitutive Relations

Most of the numerical calculations reported in this study are carried out using a rate-independent  $J_2$  isotropic hardening response for the elastic–plastic matrix between the two populations of voids. The matrix response is characterized by the following representation in uniaxial tension,

$$\varepsilon = \begin{cases} \frac{\sigma}{E}, & \text{for } \sigma \leq \sigma_y \\ \frac{\sigma_y}{E} \left( \frac{\sigma}{\sigma_y} \right)^n & \text{for } \sigma > \sigma_y \end{cases} \quad (6)$$

Here,  $E$  is Young's modulus,  $\sigma_y$  is the initial yield stress, and  $n$  is the strain-hardening exponent. In all our studies,  $\sigma_y/E = 0.004$ ,  $\nu = 0.333$  and  $n = 0.1$  are used.

And the modified Gurson model is used for the homogenized representation of secondary voids volume fraction (0.036%) over the matrix. The following constitutive equation describes the matrix behaviour

$$\left( \frac{\sigma_e}{\sigma_0} \right)^2 + 2q_1 F_s \cosh \left( q_2 \frac{3\sigma_h}{2\sigma_0} \right) - 1 - q_3 F_s^2 = 0 \quad (7)$$

where  $q$  parameters values are taken  $q_1 = 1.5$ ,  $q_2 = 1$  and  $q_3 = q_1^2$ .  $F_s$  is the current volume fraction of secondary voids and  $\sigma_0$  is the equivalent tensile flow stress in the matrix.

The mesoscopic response of the unit cell is described by the following variables,

$$\text{Equivalent stress : } \sigma_e = \sqrt{\frac{1}{2} [(\sigma_1 - \sigma_2)^2 + (\sigma_2 - \sigma_3)^2 + (\sigma_3 - \sigma_1)^2]} \quad (8)$$

$$\text{Hydrostatic stress : } \sigma_h = \frac{(\sigma_1 + \sigma_2 + \sigma_3)}{3} \quad (9)$$

$$\text{Stress Triaxiality : } T = \frac{\sigma_h}{\sigma_e} \quad (10)$$

$$\text{Equivalent strain : } E_e = \left( \frac{\sqrt{2}}{3} \right) \sqrt{(E_1 - E_2)^2 + (E_2 - E_3)^2 + (E_3 - E_1)^2} \quad (11)$$

Here,  $\sigma_1, \sigma_2$  and  $\sigma_3$  are the Cauchy stresses and  $E_1, E_2$  and  $E_3$  are the logarithmic strains in  $X_1, X_2$  and  $X_3$  direction, respectively. Numerical analyses are performed at fixed triaxiality,  $T = 1/3$ .

### 3 Results and Discussion

In this section, the numerical results obtained from finite element analysis of a unit cell containing two-scale voids are presented. As mentioned earlier, both primary and secondary voids are assumed to be present right from the beginning of the deformation history. IN all our numerical analyses, the initial volume fraction of the primary voids ( $F_{p0}$ ) and secondary voids ( $F_{s0}$ ) is taken as 2.4% and 0.036%, respectively. The two populations of voids are modelled explicitly and an assumption of plane strain deformation is made. Twenty noded hexahedral brick elements are used to discretize the quarter symmetric models. A unit thickness is assumed in the  $X_3$  direction and only one element is modelled across the thickness. Typical finite element meshes used to model the two different spatial arrangements of secondary voids, shown in Fig. 1, are presented in Fig. 2. We first present the results for the case where only primary voids exist and then analyze the influence of small secondary voids on interactions between the two-scale voids and plastic flow localization.

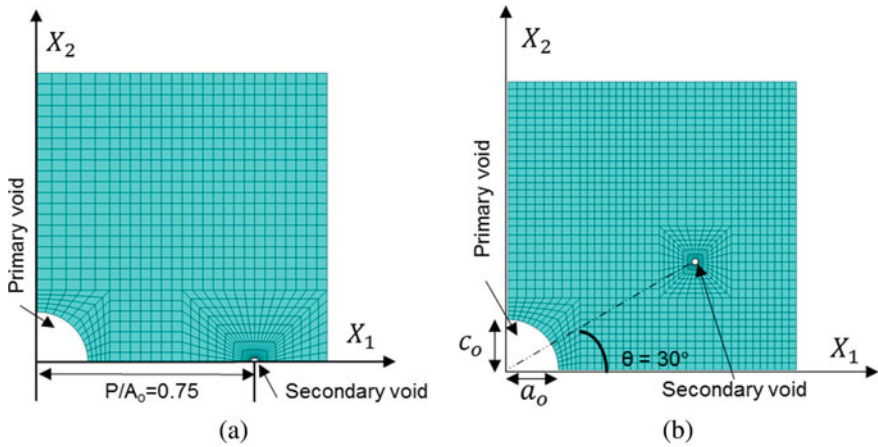


**Fig. 2** Typical finite element meshes used to discretize a quarter symmetric unit cell containing primary and secondary voids **a** Secondary void lying in the ligament between the two primary voids **b** Secondary void at an orientation of  $30^\circ$  with respect to the intervoid ligament ( $a_0$  and  $c_0$  are the undeformed radii of the primary void in  $X_1$  and  $X_2$  directions, respectively)

### 3.1 Mesoscopic Response of an Elastic–Plastic Solid Containing Only Primary Voids

The mesoscopic equivalent stress  $s$  equivalent strain response of a unit cell containing only primary void is shown in Fig. 3a. A competition between matrix material strain hardening and the porosity-induced softening can be clearly observed. Towards the later stages of the deformation history ( $E_e > 0.4$ ), the stress carrying capacity reduces abruptly. For an elastic–plastic solid containing only primary voids, the evolution of porosity is rather straightforward. Based on matrix incompressibility condition, Koplik and Needleman [11] have proposed the following relation to compute the void volume fraction  $F$ ,

$$F = 1 - (1 - F_0) \left( \frac{V_0}{V} \right) - \frac{\Delta V_e}{V} \quad (12)$$

Here,  $V_0$  and  $V$  are the initial and current volume of the unit cell, respectively, and  $F_0$  is the initial void volume fraction.  $\Delta V_e$  is the elastic dilation of the matrix resulting from the hydrostatic stress and can be obtained as

$$\Delta V_e = V_0(1 - F_0) \frac{3(1 - 2\nu)}{E} \sigma_h \quad (13)$$

The evolution of porosity obtained from the Koplik and Needleman scheme is presented in Fig. 3b. Initially, the void growth is slow, and the porosity evolution curve is varying almost linearly with the equivalent strain. As the deformation progresses, the deformation mode shifts to a uniaxial mode of straining that corresponds to flow localization in the ligament between the two adjacent voids. At this stage, the void volume fraction increases rapidly, often referred to as the onset of void coalescence, and the event is associated with a rapid drop in the load carrying capacity. An interested reader can find further details elsewhere [11]. Apart from porosity the evolution of void aspect ratio  $W$ , defined as the ratio of axial to transverse semi-axes ( $W = c/a$ ), with the equivalent strain is also analyzed, see Fig. 3c. Under uniaxial tension, the void first evolves into a prolate shape. With the onset of plastic flow localization, the void starts growing rapidly in the transverse direction with internal necking as the mode of coalescence.

### 3.2 Effect of Secondary Voids Location on Void Interactions and Plastic Flow Localization

The spatial arrangement of secondary voids shown in Fig. 1a is analyzed in this subsection. The position of primary void is kept fixed and the location of secondary void, in the intervoid ligament between the two primary voids, is varied to understand the



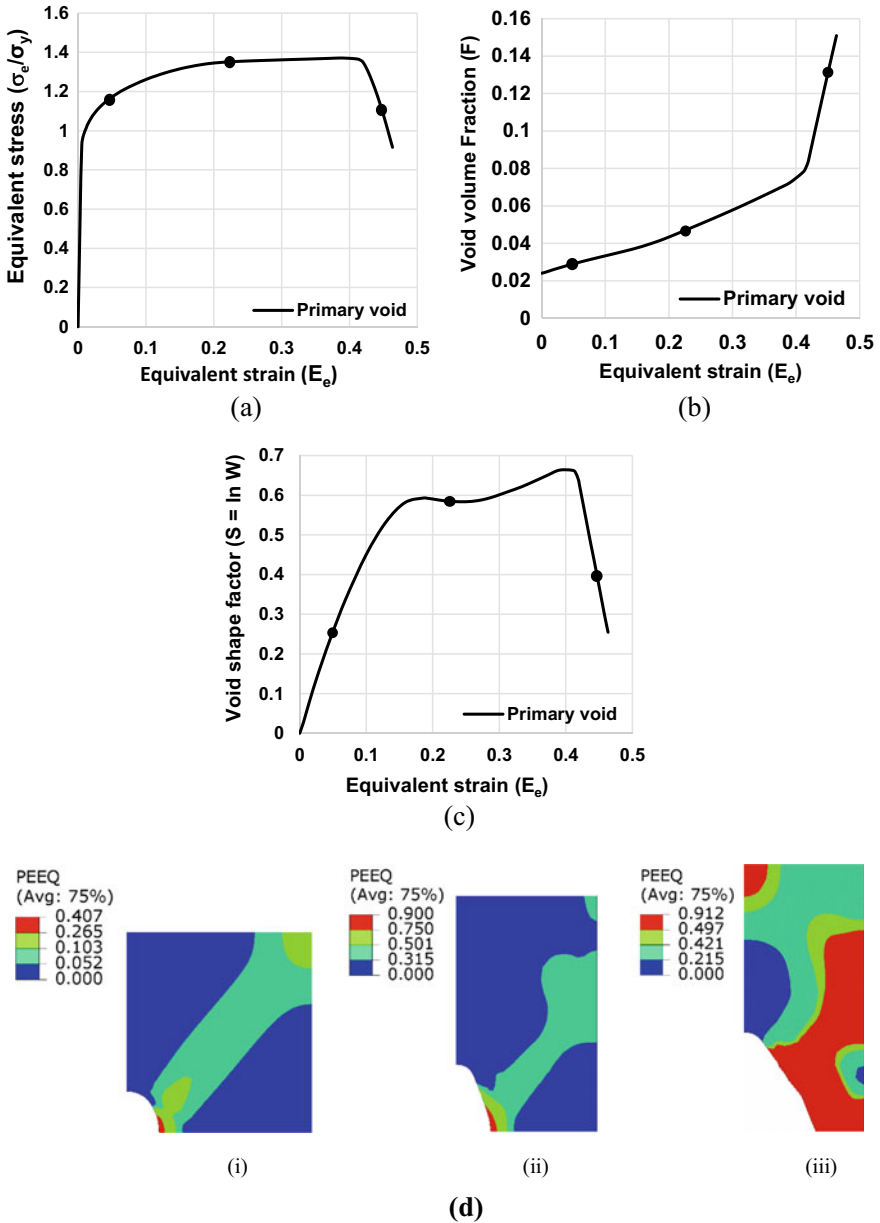


**Fig. 3** Plane strain response of a unit cell containing only primary voids ( $F_p = 0.024$ ) under a uniaxial tensile load (a) Normalized equivalent stress versus equivalent strain (b) Void volume fraction versus equivalent strain (c) Void shape versus equivalent strain (d) Contours of equivalent plastic strain at different stages in the deformation history (shown by open circle in figure a,b and c)

influence of secondary voids distribution on the interactions between the two-scale voids and plastic flow localization. The mesoscopic equivalent stress Vs equivalent strain response of the unit cell for the three different arrangements of secondary voids ( $P/A_0 = 0.25, 0.50$  and  $0.75$ ) is shown in Fig. 4a. For comparison purpose, the results for the case where only primary voids exist, presented in Sect. 3.1, are also included. For an initial void volume fraction of 0.036%, a homogenized representation of the secondary voids, using the Gurson model, lead to a very small additional constitutive softening and the mesoscopic response is almost the same as observed for the case where only primary voids exist. In contrast, the discrete representation of secondary voids has shown an interesting effect of voids distribution on the mesoscopic response. When a secondary void is located close to a primary void ( $P/A_0 = 0.25$ ), the intervoid ligament is quite small. As the voids grow, the ligament reduces, leading to the coalescence of the secondary void during the early stage of the deformation history.

Beyond this stage, the two coalesced voids start behaving like a single primary void but with a larger void volume fraction. As a result, the mesoscopic stress–strain curve deviates from that of primary voids almost right from the beginning. When  $P/A_0 = 0.5$ , initially, both the voids grow almost independent of each other. As deformation progresses, the von-mises stress around the secondary void distorts its shape. This leads to magnification of the hydrostatic stress around the primary void causing it to grow at a faster rate. The accelerated growth of the primary void generates sufficient hydrostatic stress around the secondary void, thus, enhancing the growth of the latter. This complex interaction between the two-scale voids results in a rapid evolution of total porosity. As a result, the mesoscopic response becomes soft and starts falling below that of the primary voids. With further deformations, the localization of plastic flow sets in with a consequent rapid drop in the load carrying capacity. When the distance of the secondary void from the neighbouring primary void is large ( $P/A_0 = 0.75$ ), it is basically the two secondary voids that interact with each other, and the growth of primary voids is largely uninfluenced. The mesoscopic response, therefore, is almost like that of primary voids till the localization of plastic flow starts. A plot of mesoscopic transverse strain  $E_1$  Versus equivalent strain for the three different arrangements of secondary voids is presented in Fig. 4b. Near the onset of flow localization, the deformation mode abruptly shifts to a uniaxial mode of straining and the cell transverse deformation stops. The maximum reduction in the mesoscopic ductility is observed when the secondary voids are located at the distance of  $P/A_0 = 0.5$ . Figure 4d, f shows the influence of secondary voids locations on the evolution of porosity. A numerical integration scheme was used to evaluate the primary and secondary void volume fractions separately. The accuracy of the numerical scheme was assessed by comparing the total void volume fraction ( $F_p + F_s$ ) with that obtained from the Koplik and Needleman scheme [11]. For  $P/A_0 = 0.25$ , the coalescence between primary and secondary void occurs during the early stage of the deformation process. The porosity evolution curves of the two voids are terminated at the stage of void collapse and subsequently, only the evolution of total porosity is shown. When  $P/A_0 = 0.5$ , the void collapse occurs after significant plastic deformation, and the total porosity at this stage is more than three times the

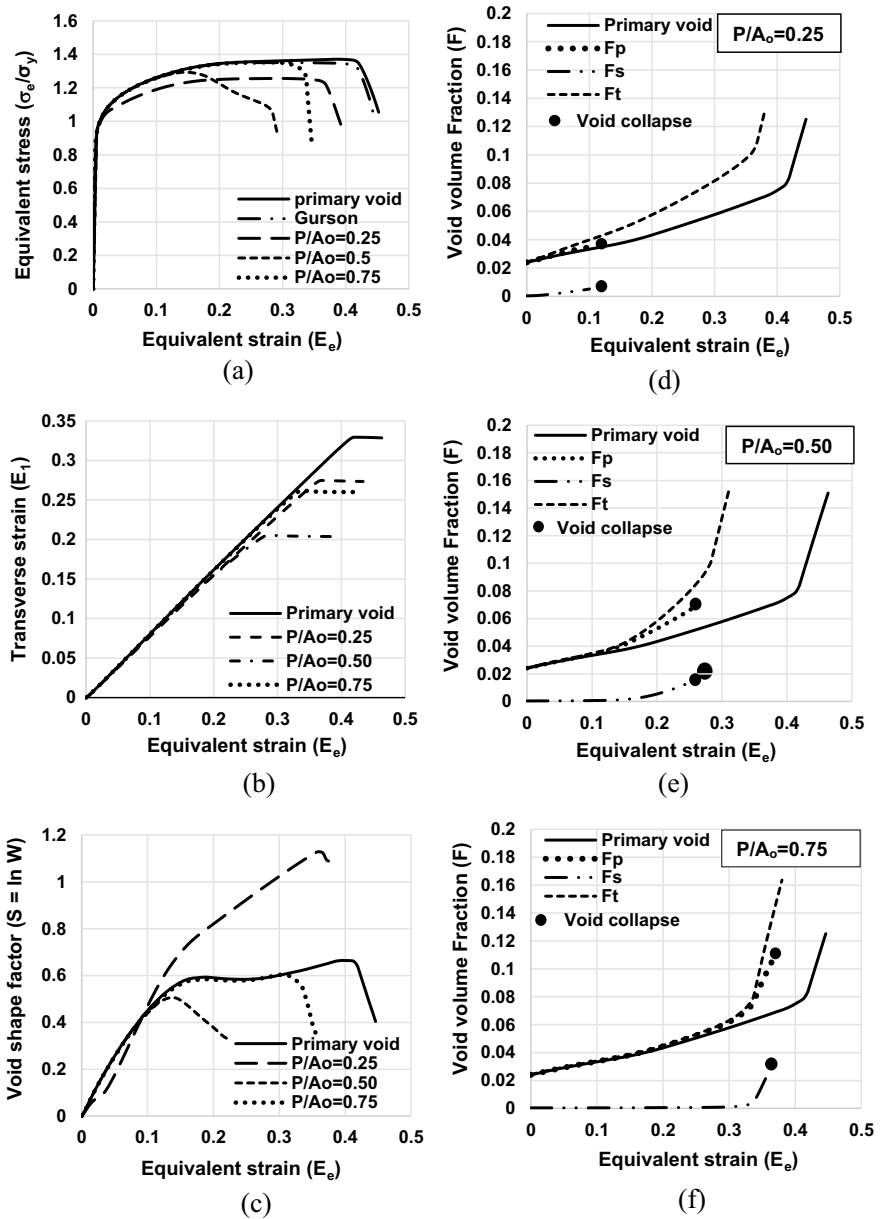


**Fig. 4** Effect of secondary voids location on **a** equivalent stress Versus equivalent strain **b** Transverse strain versus equivalent strain **c** evolution of primary void shape. The evolution of void volume fraction for  $P/A_o = 0.25, 0.5$  and  $0.75$  is shown in **d, e** and **f**, respectively. Notations  $F_p$  and  $F_s$  denote the void volume fraction of primary and secondary voids, respectively. The total void volume fraction is denoted as  $F_t$

initial porosity. When secondary void is located at a large distance  $P/A_0 = 0.75$ , the localization of plastic flow arising due to growth of the primary void accelerates the growth of the secondary void. As a result, the collapse between primary and secondary void is observed at a strain level that is higher than that required for localization of plastic flow.

The effect of secondary voids distribution on the evolution of primary void shape was also analyzed, see Fig. 4c. For  $P/A_0 = 0.25$ , the presence of a secondary void and its early coalescence results in some changes in the shape of primary voids particularly in the initial stage of deformations. Subsequently, the primary void continues to evolve into a prolate shape till the localization of plastic flow starts. When  $P/A_0 = 0.5$ , the strong interactions between the two-scale voids arrest the axial stretching of primary void and void flattening starts resulting in collapse between the primary and secondary void. For the case, where secondary voids are located at a large distance from the primary void  $P/A_0 = 0.75$ , the shape of the latter, until the commencement of flow localization, remains almost the same as observed for the case where only primary voids exist.

The effect of secondary voids distribution, in the ligament between the two primary voids, on the two-scale voids interactions is shown pictorially in Fig. 5. The plots of equivalent plastic strain for the case where only primary voids exist and the other three cases where secondary voids are at different locations in the intervoid ligament are extracted at a fixed imposed strain ( $E_2 = 0.2$ ).

### 3.3 *Effect of Secondary Voids Orientation on Void Interactions and Plastic Flow Localization*

We now examine the effect of secondary voids orientation with respect to the ligament between the two primary voids, see Fig. 1b, on the two-scale voids interaction and plastic flow localization. Since the boundary conditions imposed on the cell model exclude the possibility of bifurcation, internal necking is the only mode of void coalescence that can be simulated in our numerical studies. Nevertheless, some useful insights can still be gained by analyzing the effect of the spatial distribution of secondary voids on mesoscale plastic flow. In all the results presented in this subsection, the secondary voids are located at a fixed distance  $P/A_0 = 0.5$  and the orientation angle  $\theta$  is varied. Numerical results of mesoscopic stress–strain response, the evolution of porosity and primary void shape is presented for  $\theta = 0, 15$  and  $30^\circ$ , see Fig. 6. Results for the case  $\theta = 0^\circ$  have already been presented in the previous sub-Sect. 3.2 and are included here just for comparison's sake. As expected, the case  $\theta = 0^\circ$  leads to a maximum reduction in the mesoscopic ductility. As the angle  $\theta$  increases, the effect of secondary voids on the mesoscopic stress–strain response and porosity evolution diminishes and for  $\theta \geq 30^\circ$  it becomes almost insignificant.

It is recognized that typically the secondary voids nucleate in the regions of strain concentration arising due to flow localization in the ligament between the two

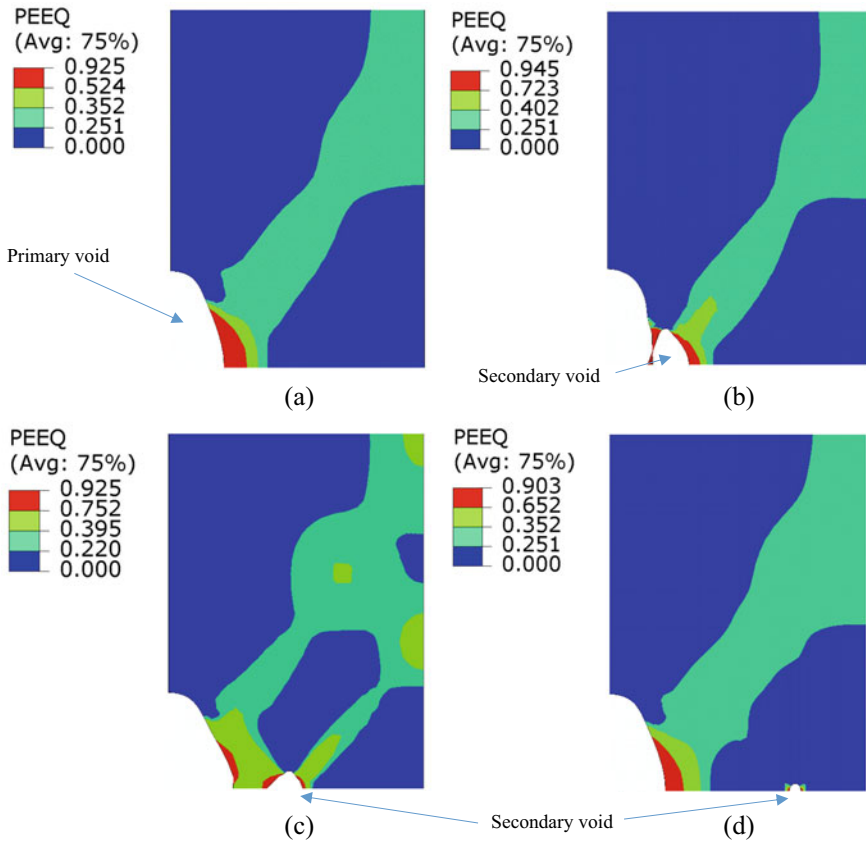


**Fig. 5** Contours of equivalent plastic strain for the case where only primary voids exist is shown in (a). The distance of the secondary void from the neighbouring primary void  $P/A_0$  is 0.25, 0.5 and 0.75 in (b), (c) and (d), respectively. The contours are extracted at a fixed value of axial strain  $E_2 = 0.2$

neighbouring primary voids. If due to local heterogeneity in the matrix or some other reason the secondary void has nucleated at an arbitrary location, then to what extent its growth may affect the macroscopic response is examined numerically.

The configuration of voids shown in Fig. 1, especially under the uniaxial loading condition, is favourable to internal necking as the mode of coalescence between the neighbouring primary voids. Initially, as the deformation increases, the tendency for shear band formation is observed. Since the kinematic constraint in our cell model analysis excludes the possibility of bifurcation, the developed stress fields around the secondary voids oriented at an angle of  $15^\circ$  and  $30^\circ$  are not strong enough to trigger the growth of voids. With further deformation, internal necking occurs between the ligament of primary voids. As a result, the secondary voids located at 0-degree

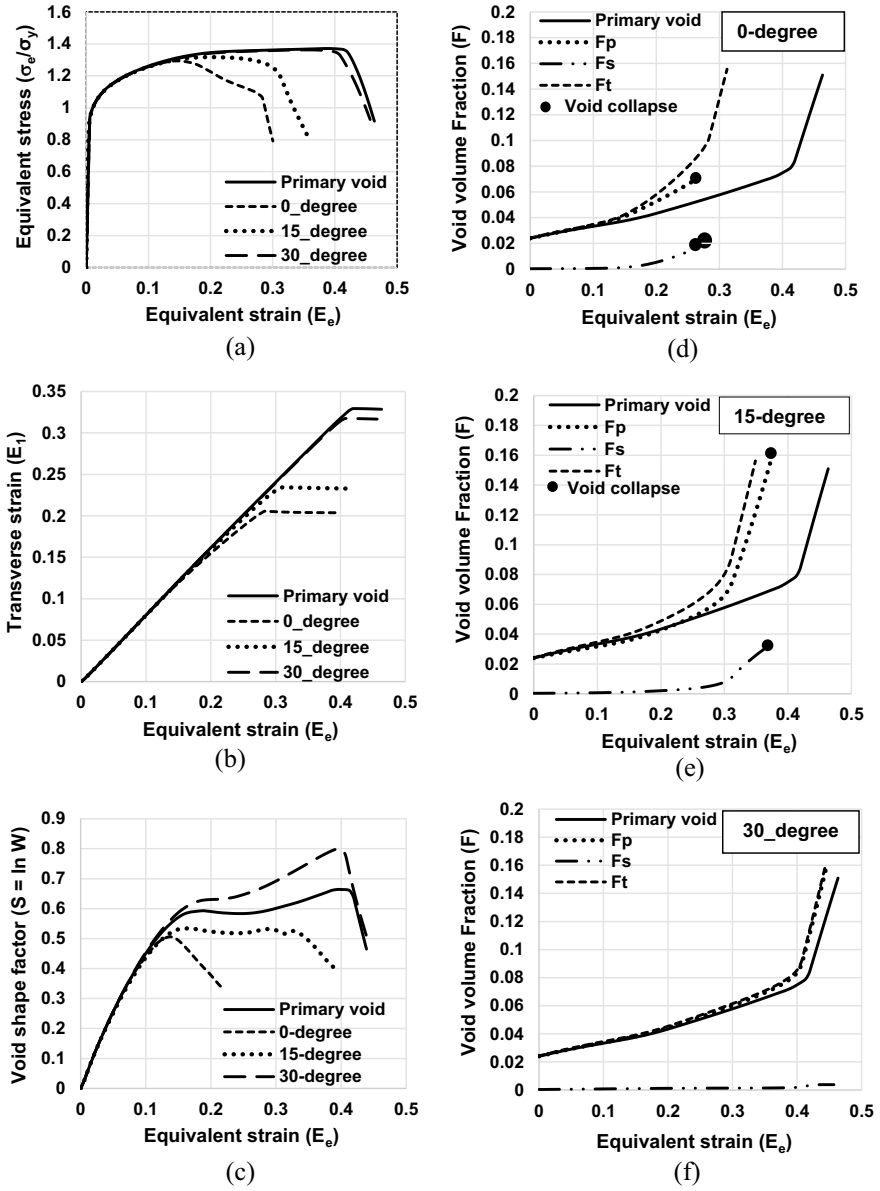


**Fig. 6** Effect of orientation of secondary voids on (a) equivalent stress versus equivalent strain (b) Transverse strain versus equivalent strain (c) evolution of primary void shape. The evolution of void volume fraction for  $P/A_0 = 0.25, 0.5$  and  $0.75$  is shown in (d), (e) and (f), respectively. Notations  $F_p$  and  $F_s$  denote the void volume fraction of primary and secondary voids, respectively. The total void volume fraction is denoted as  $F_t$

exhibits an accelerated growth, see Fig. 6d, resulting in a significant loss of stress carrying capacity and an earlier localization of plastic flow.

At  $\theta = 0^\circ$ , the secondary void is lying in the relatively higher stress triaxiality regime and, therefore, exhibits a much faster lateral growth. In fact, a physical collapse (void impingement) between primary and secondary void occurs slightly before the mesoscopic flow localization. For  $\theta = 15^\circ$ , the growth of secondary voids is comparatively slow, see Fig. 6e, and the mesoscopic flow localization occurs earlier before their physical collapse. For  $\theta = 30^\circ$ , a collapse between primary and secondary voids is not observed. It is perhaps worth discussing the influence of secondary voids orientation on their shape evolution. In general, a high stress triaxiality promotes void growth whereas void shape changes and void rotations are more prominent at low stress triaxiality. The contours of equivalent plastic strain, shown in Fig. 7, clearly show this tendency. As the orientation angle  $\theta$  increases, shear stress field around

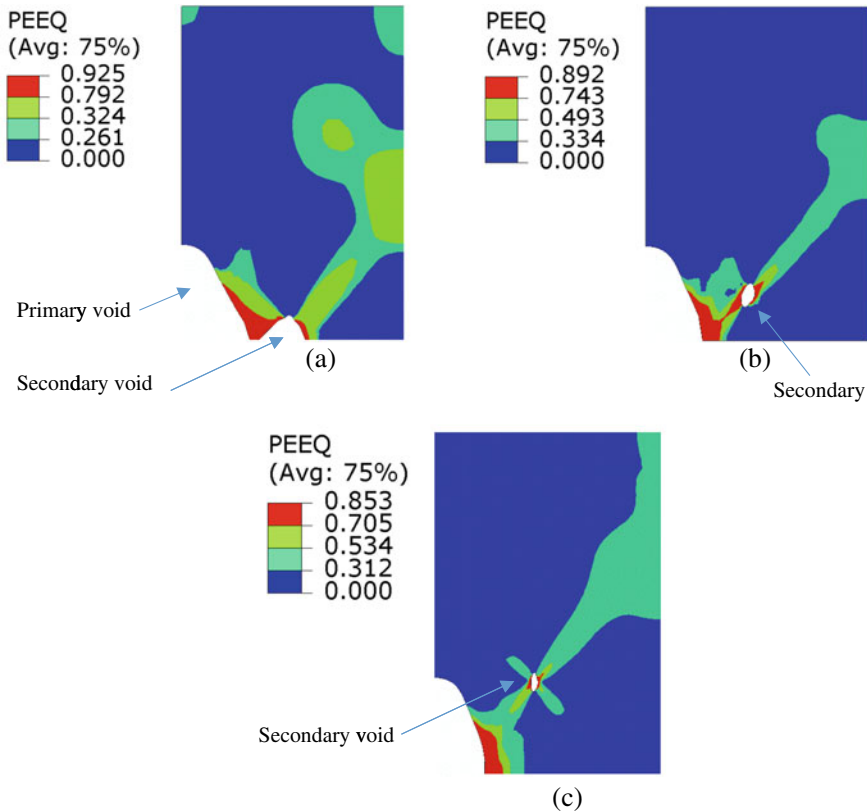


**Fig. 7** Contours of equivalent plastic strain for three different orientations of secondary voids. The secondary void is at a fixed distance ( $P/A_0 = 0.5$ ) from the primary void. The orientation angle  $\theta$  is 0, 15 and  $30^\circ$  in (a), (b) and (c), respectively. The contours are extracted at a fixed value of axial strain  $E_2 = 0.25$

the secondary void becomes significant, thus, leading to noticeable changes in shape and orientation of secondary voids.

## 4 Conclusions

The numerical results reported in this study have led to the following conclusions:

1. Secondary voids even of small initial volume fraction ( $f_{s_0}/f_{p_0} \approx 0.015$ ) may exhibit a significant influence on the evolution of porosity and, hence, on the mesoscopic ductility.
2. Depending upon the location of secondary voids in the intervoid ligament between the primary voids, a complex interaction between the two-scale voids sets in which results in a faster evolution of total porosity. In such cases, a physical collapse between the primary and secondary void is observed slightly before the onset of plastic flow localization. If the secondary voids are too near or too far from the primary voids, then it is the localization of plastic flow that accelerates the evolution of porosity.
3. For the mode of internal necking analyzed in this study, a secondary void lying in the intervoid ligament between the primary voids ( $\theta = 0^\circ$ ) leads to a maximum reduction in mesoscopic ductility.

## References

1. Tipper CF (1949) The fracture of metals 39:133–137
2. Benzerga AA, Leblond JB (2010) Ductile fracture by void growth to coalescence. *Adv Appl Mech* 44:169–305. [https://doi.org/10.1016/S0065-2156\(10\)44003-X](https://doi.org/10.1016/S0065-2156(10)44003-X)
3. Benzerga AA, Leblond JB, Needleman A, Tvergaard V (2016) Ductile failure modeling. *Int J Fract* 201:29–80. <https://doi.org/10.1007/s10704-016-0142-6>
4. McClintock (1968) A criterion for ductile fracture by the growth of holes. *J Appl Mech* 35: 363–373
5. Rice JR, Tracey DM (1969) On the ductile enlargement of voids in triaxial stress fields\*. *J Mech Phys Solids* 17:201–217. [https://doi.org/10.1016/0022-5096\(69\)90033-7](https://doi.org/10.1016/0022-5096(69)90033-7)
6. Gurson AL (1975) Plastic flow and fracture behavior of ductile materials incorporating void nucleation
7. Gurson AL (1977) Continuum theory of ductile rupture by void nucleation and growth : Part 1—Yield criteria and flow rules for porous ductile media. *J Eng Mat Tech* 2–15
8. Bao Y, Wierzbicki T (2004) On fracture locus in the equivalent strain and stress triaxiality space 46:81–98. <https://doi.org/10.1016/j.ijmecsci.2004.02.006>
9. Benzerga AA, Leblond JB, Needleman A, Tvergaard V (2016). Ductile failure modeling. <https://doi.org/10.1007/s10704-016-0142-6>
10. Morin L, Leblond JB, Tvergaard V (2016) Application of a model of plastic porous materials including void shape effects to the prediction of ductile failure under shear-dominated loadings. *J Mech Phys Solids* 94:148–166. <https://doi.org/10.1016/j.jmps.2016.04.032>
11. Koplik J, Needleman A (1988) Void growth and coalescence in porous. *Int J Solids Struct* 24:835–853. [https://doi.org/10.0020-7683\(88\)90051-0](https://doi.org/10.0020-7683(88)90051-0)



12. Rice JR (1976) The localization of plastic deformation. 14th international congress on theoretical applied mechanics. 207–220. <https://doi.org/10.1.1.160.6740>
13. Needleman A, Rice JR (1978) Limits to ductility set by plastic flow localization 44:262–270
14. Perrin G, Leblond JB (2000) Accelerated void growth in porous ductile solids containing two populations of cavities. *Int J Plast* 16:91–120. [https://doi.org/10.1016/S0749-6419\(99\)00049-2](https://doi.org/10.1016/S0749-6419(99)00049-2)
15. Brocks W, Sun DZ, Hönl A (1995) Verification of the transferability of micromechanical parameters by cell model calculations with visco-plastic materials. *Int J Plast* 11:971–989. [https://doi.org/10.1016/S0749-6419\(95\)00039-9](https://doi.org/10.1016/S0749-6419(95)00039-9)
16. Fabrègue D, Pardoën T (2008) A constitutive model for elastoplastic solids containing primary and secondary voids. *J Mech Phys Solids* 56:719–741. <https://doi.org/10.1016/j.jmps.2007.07.008>
17. Gao X, Kim J (2006) Modeling of ductile fracture: significance of void coalescence. *Int J Solids Struct* 43:6277–6293. <https://doi.org/10.1016/j.ijsolstr.2005.08.008>
18. Faleskog J, Shih CF (1996) Micromechanics of coalescence: Synergism between elasticity, plastic yielding and multi-size scale voids. *J Phys IV JP*. 6. <https://doi.org/10.1051/jp4:1996609>.
19. Tvergaard V (1996) Effect of void size difference on growth and cavitation instabilities. *J Mech Phys Solids* 44:1237–1253. [https://doi.org/10.1016/0022-5096\(96\)00032-4](https://doi.org/10.1016/0022-5096(96)00032-4)
20. Tvergaard V (1998) Interaction of very small voids with larger voids. *Int J Solids Struct* 35:3989–4000
21. Wen J, Huang Y, Hwang KC, Liu C, Li M (2005) The modified Gurson model accounting for the void size effect. *Int J Plast* 21:381–395. <https://doi.org/10.1016/j.ijplas.2004.01.004>
22. Peerlings RHJ, Poh LH, Geers MGD (2012) An implicit gradient plasticity-damage theory for predicting size effects in hardening and softening. *Eng Fract Mech* 95:2–12. <https://doi.org/10.1016/j.engfracmech.2011.12.016>
23. Monchiet V, Bonnet G (2013) A Gurson-type model accounting for void size effects. *Int J Solids Struct* 50:320–327. <https://doi.org/10.1016/j.ijsolstr.2012.09.005>
24. Hütter G, Zymbell L, Kuna M (2014) Size effects due to secondary voids during ductile crack propagation. *Int J Solids Struct* 51:839–847. <https://doi.org/10.1016/j.ijsolstr.2013.11.012>
25. Zymbell L, Hütter G, Linse T, Mühlich U, Kuna M (2014) Size effects in ductile failure of porous materials containing two populations of voids. *Eur J Mech A/Solids* 45:8–19. <https://doi.org/10.1016/j.euromechsol.2013.11.006>
26. Khan IA, Bhasin V (2017) On the role of secondary voids and their distribution in the mechanism of void growth and coalescence in porous plastic solids. *Int J Solids Struct* 108:203–215. <https://doi.org/10.1016/j.ijsolstr.2016.12.016>
27. Tvergaard V (2009) Behaviour of voids in a shear field. *Int J Fract* 158:41–49. <https://doi.org/10.1007/s10704-009-9364-1>